



Published in final edited form as:

J Am Chem Soc. 2019 January 09; 141(1): 94–97. doi:10.1021/jacs.8b11441.

TiO₂ Nanoparticles Catalyze Oxidation of Huntingtin Exon 1-Derived Peptides Impeding Aggregation: A Quantitative NMR Study of Binding Kinetics

Alberto Ceccon, Vitali Tugarinov*, and G. Marius Clore*

Laboratory of Chemical Physics, National Institute of Diabetes and Digestive and Kidney Diseases, National Institutes of Health, Bethesda, Maryland 20892-0520, United States

Abstract

Polyglutamine expansion within the N-terminal region of the huntingtin protein results in the formation of intracellular aggregates responsible for Huntington's disease, a fatal neurodegenerative condition. The interaction between TiO₂ nanoparticles and huntingtin peptides comprising the N-terminal amphiphilic domain without (htt^{NT}) or with (htt^{NT}Q₁₀) a ten-residue C-terminal polyglutamine tract, is investigated by NMR spectroscopy. TiO₂ nanoparticles decrease aggregation of htt^{NT}Q₁₀ by catalyzing the oxidation of Met⁷ to a sulfoxide, resulting in an aggregation-incompetent peptide. The oxidation agent is hydrogen peroxide generated on the surface of the TiO₂ nanoparticles either by UV irradiation or at low steady-state levels in the dark. The binding kinetics of nonaggregating htt^{NT} to TiO₂ nanoparticles is characterized by quantitative analysis of ¹⁵N dark state exchange saturation transfer and lifetime line broadening NMR data. Binding involves a sparsely populated intermediate that experiences hindered rotational diffusion relative to the free state. Catalysis of methionine oxidation within the N-terminal domain of the huntingtin protein may potentially provide a strategy for delaying the onset of Huntington's disease.

Polyglutamine expansion within the N-terminal region of the huntingtin protein (corresponding to exon-1) favors aggregation and is responsible for Huntington's disease, a fatal neurodegenerative condition.¹ The polyglutamine domain lies downstream of the 16-residue N-terminal amphiphilic domain (htt^{NT}). Peptides comprising htt^{NT} with as few as 10 glutamines (htt^{NT}Q₁₀) aggregate rapidly in solution and form polymorphic fibrils.² We recently observed that oxidation of the Met⁷ side-chain to a sulfoxide (Met⁷) prevents aggregation of htt^{NT}Q₁₀.³ In general, adsorption of fibril forming proteins and peptides on the surface of nanoparticles enhances aggregation and fibril formation by increasing the local peptide concentration and hence the probability of forming a critical initiation nucleus.^{4,5} Titanium oxide nanoparticles (TiO₂ NPs) are unique as they possess photocatalytic properties that generate reactive oxygen species upon UV irradiation.^{6,7} Here we study the interaction of htt^{NT} and htt^{NT}Q₁₀ with TiO₂ NPs by NMR, and show that TiO₂ NPs

*Corresponding Authors mariusc@mail.nih.gov. *vitali.tugarinov@nih.gov.

Notes

The authors declare no competing financial interest.

specifically catalyze the oxidation of Met7, thereby preventing fibril formation by reducing the concentration of the aggregation-competent, native reduced form of htt^{NT}Q₁₀.

Spontaneous aggregation of htt^{NT}Q₁₀ occurs over time as monitored both by an increase in Thioflavin T (ThT) fluorescence emission (Figure 1A), attributed to the formation of β -rich amyloid-like structures, and by a decrease in the intensity of the amide proton envelope of the NMR signal (Figure 1B; see SI). Reduced and oxidized monomeric htt^{NT}Q₁₀ are NMR visible, while aggregates of reduced htt^{NT}Q₁₀ are broadened beyond detection, resulting in a decrease in the observable amide proton envelope intensity. Addition of photoexcited TiO₂ NPs (see SI and Figure S1) dramatically reduces the extent of aggregation. At 10 °C, only 8% of a 300 μ M ¹⁵N-htt^{NT}Q₁₀ sample remains NMR visible after 100 h; in the presence of photoexcited TiO₂ NPs, however, aggregation plateaus out with 33% of the sample remaining NMR visible (Figure 1B). The apparent aggregation $t_{1/2}$ (~23–25 h), however, is not affected by the TiO₂ NPs (Figure 1B). The reduction in the fraction of aggregating species can be attributed to TiO₂ NP catalyzed oxidation of the side chain of Met⁷ to a sulfoxide. Several reactive oxygen species are formed on the surface of TiO₂ NPs upon UV irradiation (Figure S2),^{6,7} but only H₂O₂ is stable with significant amounts generated both upon UV irradiation and in the dark (Figures 2A and S3).

The oxidation kinetics of htt^{NT}Q_{*n*} huntingtin peptides (where *n* = number of glutamines in the polyglutamine tract) in the presence of TiO₂ NPs can be described by three parallel reactions (Scheme 1): two second-order processes involving oxidation of htt^{NT}Q_{*n*} (P_{red}) to Met⁷O-htt^{NT}Q_{*n*} (P_{oxi}) by H₂O₂, generated upon UV irradiation, either dissolved in solution (k_1) or on the surface of the TiO₂ NPs (k_2), and a pseudo-first-order process ($k_3^{\text{dark}} = k_2[\text{H}_2\text{O}_2]_{\text{dark}}$) occurring in the dark that involves a low steady-state (i.e., continuously generated) level of H₂O₂ on the surface of the TiO₂ NPs.⁸ These reactions occur concomitantly with aggregation of P_{red} which, for simplicity, is described as a unimolecular process with a rate constant k_{agg} . Our treatment of the kinetics of all oxidative processes assumes that oxidation proceeds on a time-scale much slower than that of binding to TiO₂ NPs, as is amply confirmed experimentally (see below).

To study the kinetics of TiO₂ catalyzed oxidation of huntingtin peptides in the absence of aggregation ($k_{\text{agg}} = 0$ in Scheme 1), we made use of a peptide comprising only the N-terminal amphiphilic domain, htt^{NT}, which remains stable in the presence of TiO₂ NPs for many days (Figure S4). Oxidation of htt^{NT} by H₂O₂ free in solution makes an insignificant contribution to the kinetics of htt^{NT} oxidation in the presence of 5 g·L⁻¹ TiO₂ NPs as the concentration of dissolved H₂O₂ generated upon UV irradiation (~11 μ M, Figure 2A) is 10-fold lower than that used in the experiment with added H₂O₂ shown in Figure 2B. The time course of oxidation in the presence of UV irradiated TiO₂ is biphasic (Figure 2C). The first phase arises from second-order ($k_2 \sim 500 \text{ M}^{-1} \text{ h}^{-1}$) oxidation of Met⁷ by the substantial amount of H₂O₂ located on the surface of the TiO₂ NPs generated by UV irradiation. Oxidation on the TiO NP surface is accelerated ~45-fold relative to that free in solution. Once H₂O₂ generated by UV irradiation is consumed, a slower apparent first order oxidation process ($k_3^{\text{dark}} = k_2[\text{H}_2\text{O}_2]_{\text{dark}} \sim 0.002 \text{ h}^{-1}$) occurs owing to the steady-state level of H₂O₂

present on the TiO₂ NP surface in the dark. With these values of k_2 and k_3^{dark} , Scheme 1 quantitatively accounts for the disappearance of NMR visible htt^{NT}Q₁₀ in the presence of photoactivated TiO₂ NPs with $k_{\text{agg}} \sim 0.03 \text{ h}^{-1}$ which remains unchanged in the absence of TiO₂ NPs (Figure 1B).

The efficiency of heterogeneous catalysis is dependent upon the strength of interaction between the adsorbate (htt^{NT}) and the surface of the catalyst.⁹ We therefore characterized the kinetic and mechanistic details of ¹⁵N-labeled htt^{NT} adsorption on the surface of TiO₂ NPs using ¹⁵N dark state exchange saturation transfer (DEST) and lifetime line broadening (R_2) which enable one to quantitatively analyze exchange processes between an NMR visible species and very high molecular weight, NMR invisible “dark” states.^{10–13} Although binding of httNTQ₁₀ to TiO₂ NPs cannot be studied quantitatively owing to httNTQ₁₀ aggregation during the time course of the DEST experiment (several days), R_2 measurements are sufficiently fast (a few hours) to demonstrate significant ¹⁵N lifetime line broadening ($\sim 10 \text{ s}^{-1}$), and hence binding, of httNTQ₁₀ in the presence of TiO NPs (Figure S5).

Examples of ¹⁵N-DEST profiles and a plot of ¹⁵N- R_2 as a function of residue for reduced htt^{NT} in the presence of TiO₂ NPs in the dark are shown in Figure 3A,B, respectively. These conditions correspond to a quasi-equilibrium state where Met⁷ oxidation by the small amount of steady-state H₂O₂ generated on the TiO₂ NP surface in the dark proceeds very slowly ($t_{1/2} \sim 350 \text{ h}$). The shapes of the ¹⁵N-DEST profiles are unusual and characterized by a narrow component superimposed on a broad one (Figure 3A) indicative of a three-state exchanging system in which the slow exchange process due to htt^{NT} binding to the TiO₂ NP surface is accompanied by a second exchange process occurring on a much faster time scale. The ¹⁵N-DEST and R_2 data were fit simultaneously to the three-state exchange model shown in red in Figure 3B via propagation of a set of Bloch-McConnell¹⁴ equations.

Exchange between free (P_F^{red}) and TiO₂ NP-bound (P_B^{red}) htt^{NT} monomer proceeds via an intermediate (P_R^{red}) whose rotational diffusion is only partially restricted, presumably due to initial binding to the hydration layer surrounding the TiO₂ NP; the final bound state experiences the same rotational diffusion as the TiO₂ NP itself (Figure 4). This binding mechanism is similar to that observed for the adsorption of cholic acid to ceria NPs.¹⁵

The population ($p_B^{\text{red}} = 1.7 \pm 0.1\%$) of TiO₂ NP-bound reduced htt^{NT}, the rate constant k_{BR} ($97 \pm 5 \text{ s}^{-1}$) for the transition from fully bound to partially restricted states, and the transverse relaxation rates in the bound state ($\langle {}^{15}\text{N-}R_2^{\text{bound}} \rangle = 31\,000 \pm 300 \text{ s}^{-1}$) are well-defined from the fits. The population of the intermediate state (P_R^{red}), however, cannot be determined with certainty without assumptions regarding the magnitude of its transverse spin relaxation rate, ${}^{15}\text{N-}R_2^{\text{restricted}}$. This is due to fast interconversion between (P_F^{red}) and (P_R^{red}) on the relaxation time-scale ($k_{\text{FR}} + k_{\text{RF}} \gg R_2^{\text{restricted}}$), so that extraction of k_{FR} , k_{RF} and ${}^{15}\text{N-}R_2^{\text{restricted}}$ is not possible without assumptions regarding these parameters. Thus,

only ranges of $^{15}\text{N-R}_2^{\text{restricted}}$ and $(p_{\text{R}}^{\text{red}})$ could be established (see SI): for $\langle ^{15}\text{N-R}_2^{\text{restricted}} \rangle = 200$ to 750 s^{-1} , $p_{\text{R}}^{\text{red}}$ varies from 0.5 to 0.2%. Although populated at less than 1%, the inclusion of $(p_{\text{R}}^{\text{red}})$ into the analysis is essential to reproduce the experimental $^{15}\text{N-DEST}$ profiles.

The $^{15}\text{N-DEST/ R}_2$ data for Leu³ and the C-terminal three residues of htt^{NT} required a separate treatment and were fitted to the three-state model shown in gray in Figure 3B. Although formally the same overall three-state exchange model is used for these residues ($p_{\text{F}}^{\text{red}} \leftrightarrow p_{\text{R}}^{\text{red}} \leftrightarrow p_{\text{T}}^{\text{red}}$), the exchange process subsumes initial binding to the NP surface followed by reversible detachment from the surface (state $(p_{\text{T}}^{\text{red}})$, where “T” denotes “tethered”).¹³ The rate constants k_{BT} and k_{TB} were calculated *a-posteriori* (see SI and Figure 4) and fall in the ranges 40 to 75 s^{-1} and 160 to 240 s^{-1} , respectively, depending on the assumed population of state $(p_{\text{R}}^{\text{red}})$. It follows that reversible detachment of these 4 residues from the NP surface occurs ~ 3 -fold slower than the binding event proper ($p_{\text{R}}^{\text{red}} \leftrightarrow p_{\text{B}}^{\text{red}}$). While the central residues of htt^{NT} are likely to form an ordered helical structure when bound to TiO₂ NPs, as observed for htt^{NT}Q_n peptides bound to lipid micelles,³ the parts of the peptide that remain unstructured in the bound state retain the flexibility of the free peptide and can transiently detach from the NP surface (i.e., they are “tethered”). The same phenomenon was also observed in the interaction of htt^{NT}Q_n with small unilamellar lipid vesicles.¹³

The binding of Met⁷O-htt^{NT} to TiO₂ NPs was also characterized by analysis of $^{15}\text{N-DEST}$ and R_2 data (Figure S6). The population of the bound state $p_{\text{B}}^{\text{oxi}}$ is $\sim 0.6\%$, ~ 3 -fold lower than that of the reduced form, indicating that oxidation of Met⁷ reduces the binding affinity to TiO₂ NPs, in agreement with previous studies on the interaction of htt^{NT}Q₇ with lipid micelles.³

In conclusion, the current work provides a mechanistic basis for understanding the interaction of huntingtin peptides with TiO₂ NPs coupled with surface-catalyzed oxidation, and suggests that targeted catalysis of Met⁷ oxidation within the htt^{NT} domain of the huntingtin protein may provide a strategy for delaying the onset of Huntington’s disease.

Supplementary Material

Refer to Web version on PubMed Central for supplementary material.

ACKNOWLEDGMENTS

We thank James Baber, Dan Garrett and Jinfa Ying for NMR and computational support. This work was supported by the Intramural Research Program of the National Institute of Diabetes and Digestive and Kidney Diseases, NIH (to G.M.C.).

REFERENCES

- (1). Andresen JM; Gayan J; Djousse L; Roberts S; Brocklebank D; Cherny SS; Cardon LR; Gusella JF; MacDonald ME; Myers RH; Housman DE; Wexler NS The Relationship between Cag Repeat Length and Age of Onset Differs for Huntington's Disease Patients with Juvenile Onset or Adult Onset. *Ann. Hum. Genet* 2007, 71, 295–301. [PubMed: 17181545]
- (2). Jayaraman M; Kodali R; Sahoo B; Thakur AK; Mayasundari A; Mishra R; Peterson CB; Wetzel R Slow Amyloid Nucleation Via α Helix-Rich Oligomeric Intermediates in Short Polyglutamine-Containing Huntingtin Fragments. *J. Mol. Biol* 2012, 415, 881–99. [PubMed: 22178474]
- (3). Ceccon A; Schmidt T; Tugarinov V; Kotler SA; Schwieters CD; Clore GM Interaction of Huntingtin Exon-1 Peptides with Lipid-Based Micellar Nanoparticles Probed by Solution NMR and Q-Band Pulsed EPR. *J. Am. Chem. Soc* 2018, 140, 6199–6202. [PubMed: 29727175]
- (4). Linse S; Cabaleiro-Lago C; Xue WF; Lynch I; Lindman S; Thulin E; Radford SE; Dawson KA Nucleation of Protein Fibrillation by Nanoparticles. *Proc. Natl. Acad. Sci. U. S. A* 2007, 104, 8691–6. [PubMed: 17485668]
- (5). Wu WH; Sun X; Yu YP; Hu J; Zhao L; Liu Q; Zhao YF; Li YM TiO₂ Nanoparticles Promote β -Amyloid Fibrillation in Vitro. *Biochem. Biophys. Res. Commun* 2008, 373, 315–8. [PubMed: 18571499]
- (6). Schneider J; Matsuoka M; Takeuchi M; Zhang J; Horiuchi Y; Anpo M; Bahnemann DW Understanding TiO₂ Photocatalysis: Mechanisms and Materials. *Chem. Rev* 2014, 114, 9919–86. [PubMed: 25234429]
- (7). Nosaka Y; Nosaka AY Generation and Detection of Reactive Oxygen Species in Photocatalysis. *Chem. Rev* 2017, 117, 11302–11336. [PubMed: 28777548]
- (8). Jayaram DT; Runa S; Kemp ML; Payne CK Nanoparticle-Induced Oxidation of Corona Proteins Initiates an Oxidative Stress Response in Cells. *Nanoscale* 2017, 9, 7595–7601. [PubMed: 28537609]
- (9). Schauermaier S; Nilius N; Shaikhtudinov S; Freund HJ Nanoparticles for Heterogeneous Catalysis: New Mechanistic Insights. *Acc. Chem. Res* 2013, 46, 1673–1681. [PubMed: 23252628]
- (10). Fawzi NL; Ying J; Torchia DA; Clore GM Kinetics of Amyloid Beta Monomer-to-Oligomer Exchange by NMR Relaxation. *J. Am. Chem. Soc* 2010, 132, 9948–9951. [PubMed: 20604554]
- (11). Fawzi NL; Ying J; Ghirlando R; Torchia DA; Clore GM Atomic-Resolution Dynamics on the Surface of Amyloid β Protofibrils Probed by Solution NMR. *Nature* 2011, 480, 268–272. [PubMed: 22037310]
- (12). Ceccon A; Tugarinov V; Bax A; Clore GM Global Dynamics and Exchange Kinetics of a Protein on the Surface of Nanoparticles Revealed by Relaxation-Based Solution NMR Spectroscopy. *J. Am. Chem. Soc* 2016, 138, 5789–5792. [PubMed: 27111298]
- (13). Ceccon A; Clore GM; Tugarinov V Decorrelating Kinetic and Relaxation Parameters in Exchange Saturation Transfer NMR: A Case Study of N-Terminal Huntingtin Peptides Binding to Unilamellar Lipid Vesicles. *J. Phys. Chem. B* 2018, 10.1021/acs.jpcc.8b07112.
- (14). McConnell HM Reaction Rates by Nuclear Magnetic Resonance. *J. Chem. Phys* 1958, 28, 430–431.
- (15). Egner TK; Naik P; Nelson NC; Slowing II; Venditti V Mechanistic Insight into Nanoparticle Surface Adsorption by Solution NMR Spectroscopy in an Aqueous Gel. *Angew. Chem., Int. Ed* 2017, 56, 9802–9806.

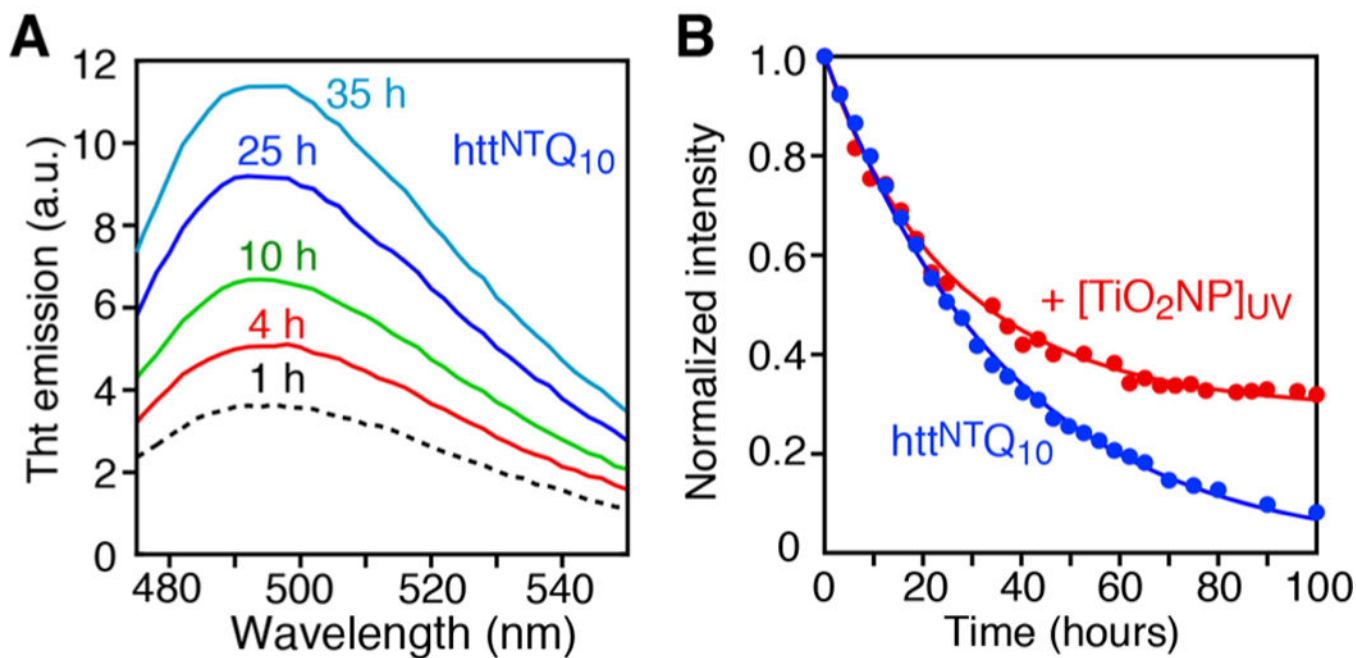


Figure 1.

Effect of TiO_2 NPs on aggregation of $\text{htt}^{\text{NTQ}}_{10}$ monitored by NMR at 10°C . Time course of (A) ThT emission of $25\ \mu\text{M}$ $\text{htt}^{\text{NTQ}}_{10}$ in the absence of TiO_2 NPs, and (B) of the intensity of the amide proton envelope of $300\ \mu\text{M}$ ^{15}N -labeled $\text{htt}^{\text{NTQ}}_{10}$ in the absence (blue circles) and presence (red circles) of $5\ \text{g}\cdot\text{L}^{-1}$ TiO_2 NPs photoexcited by exposure to UV light prior to addition to the peptide solution. The solid lines represent best fits where the disappearance of reduced, NMR visible $\text{htt}^{\text{NTQ}}_{10}$ ($k_{\text{agg}} \sim 0.03\ \text{h}^{-1}$) due to aggregation competes with oxidation to aggregation-incompetent $\text{Met}^7\text{O-htt}^{\text{NTQ}}_{10}$ (see Scheme 1). The normalized intensities are corrected for sample to sample variations in the amounts of $\text{Met}^7\text{O-htt}^{\text{NTQ}}_{10}$ present at $t = 0$ (see SI).

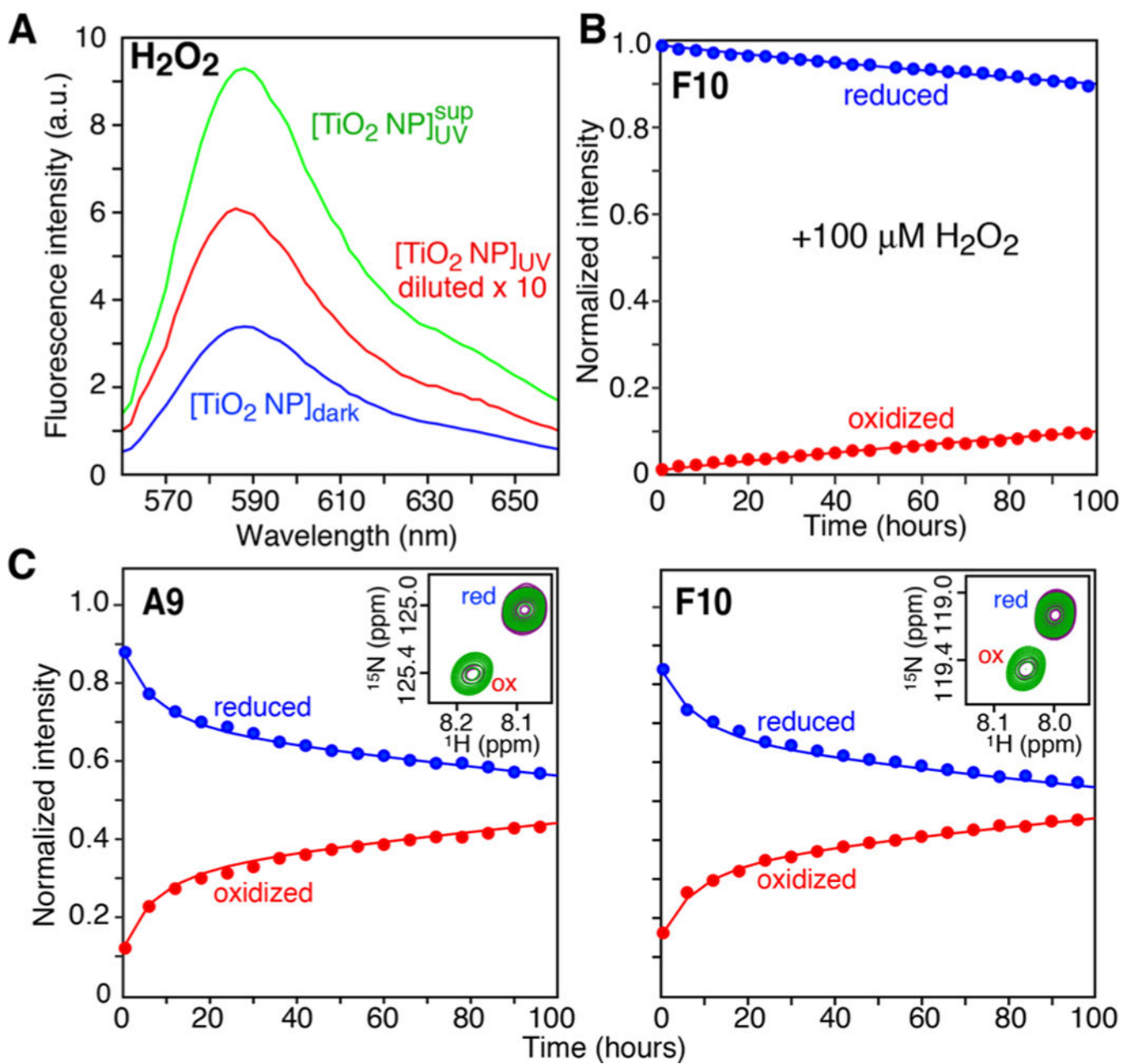


Figure 2.

TiO_2 -catalyzed oxidation of httNT. (A) Amplex Red assay for H_2O_2 generated by $5 \text{ g}\cdot\text{L}^{-1}$ TiO_2 NPs in the dark (blue, $\sim 4 \mu\text{M}$ H_2O_2) and upon UV exposure for 3 h (red, NP suspension, $\sim 76 \mu\text{M}$ H_2O_2 ; green, supernatant after removal of NPs, $\sim 11 \mu\text{M}$ H_2O_2). (B) Time course of Met⁷ oxidation of $300 \mu\text{M}$ ^{15}N -labeled httNT following addition of (B) $100 \mu\text{M}$ H_2O_2 and (C) UV-irradiated TiO_2 NPs ($5 \text{ g}\cdot\text{L}^{-1}$, 3 h UV exposure) monitored by the reduction and corresponding increase in intensities of Ala⁹ and Phe¹⁰ cross-peaks arising from reduced (blue) and Met⁷O oxidized (red) httNT, respectively, in a series of ^1H – ^{15}N HSQC spectra. The insets in (C) show the cross-peaks corresponding to the reduced (upfield) and oxidized (downfield) states at $t = 0$ (purple) and 80 (green) hours. The

experimental data in panels B and C are shown as circles and the best-fit curves obtained by nonlinear optimization and integration of the differential equations (eq S1) describing the oxidation process in Scheme 1 are represented by solid lines. The different ratios of oxidized to reduced htt^{NT} at time zero in panels (B) and (C) reflect sample to sample variations. Data were collected at 10 °C and a spectrometer frequency of 600 MHz.

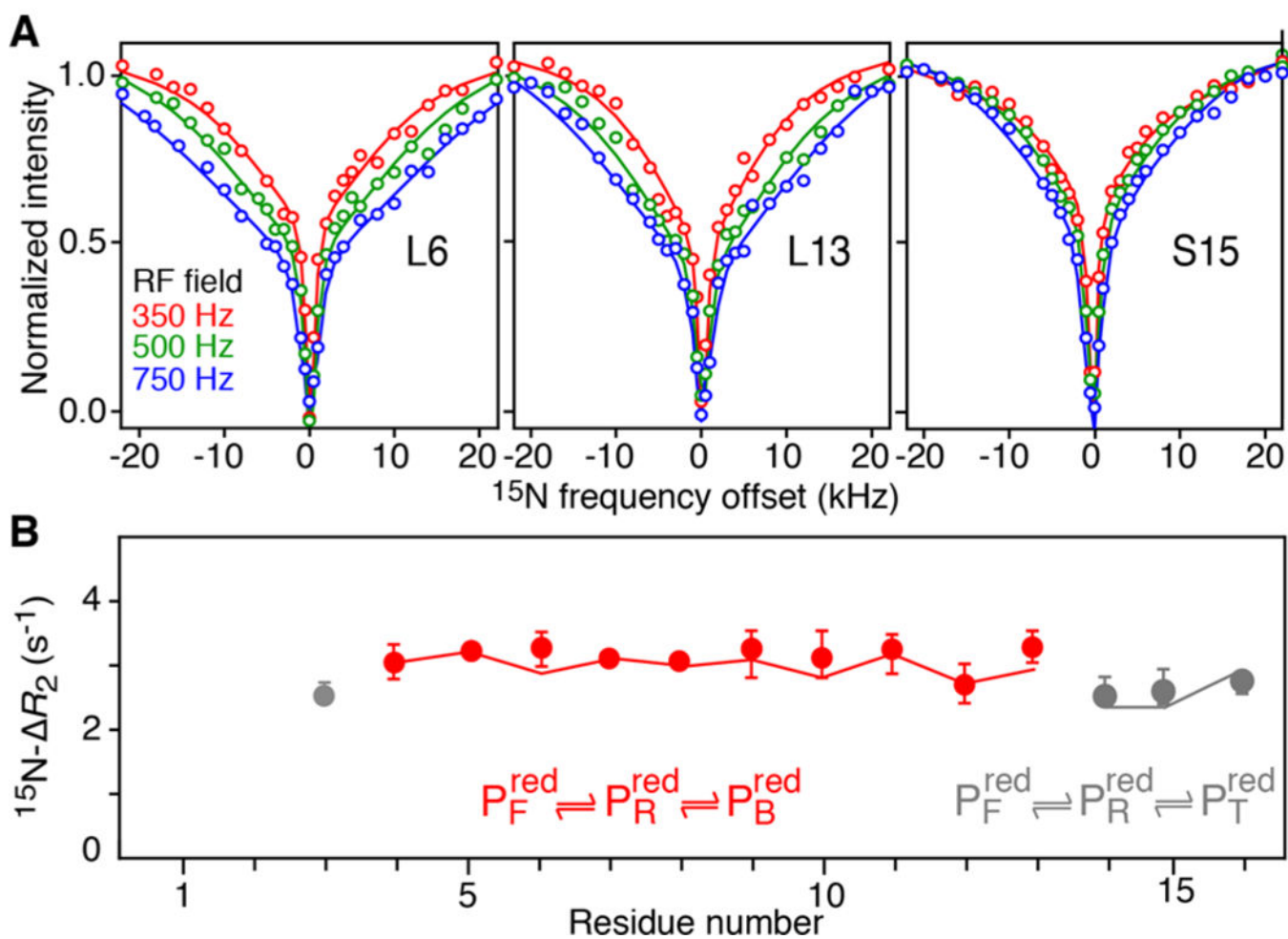


Figure 3. Kinetics of htt^{NT} binding to TiO₂ NPs characterized by relaxation-based NMR. (A) Examples of ¹⁵N-DEST profiles and (B) ¹⁵N- R_2 as a function of residue observed for 300 μM ¹⁵N-labeled htt^{NT} in the presence of 5 g·L⁻¹ TiO₂ NPs in the dark. Circles represent experimental data, and solid lines are best fits to a three-state exchange model. Residues requiring a separate treatment are shown in gray. Data were recorded at 600 MHz and 10 °C.

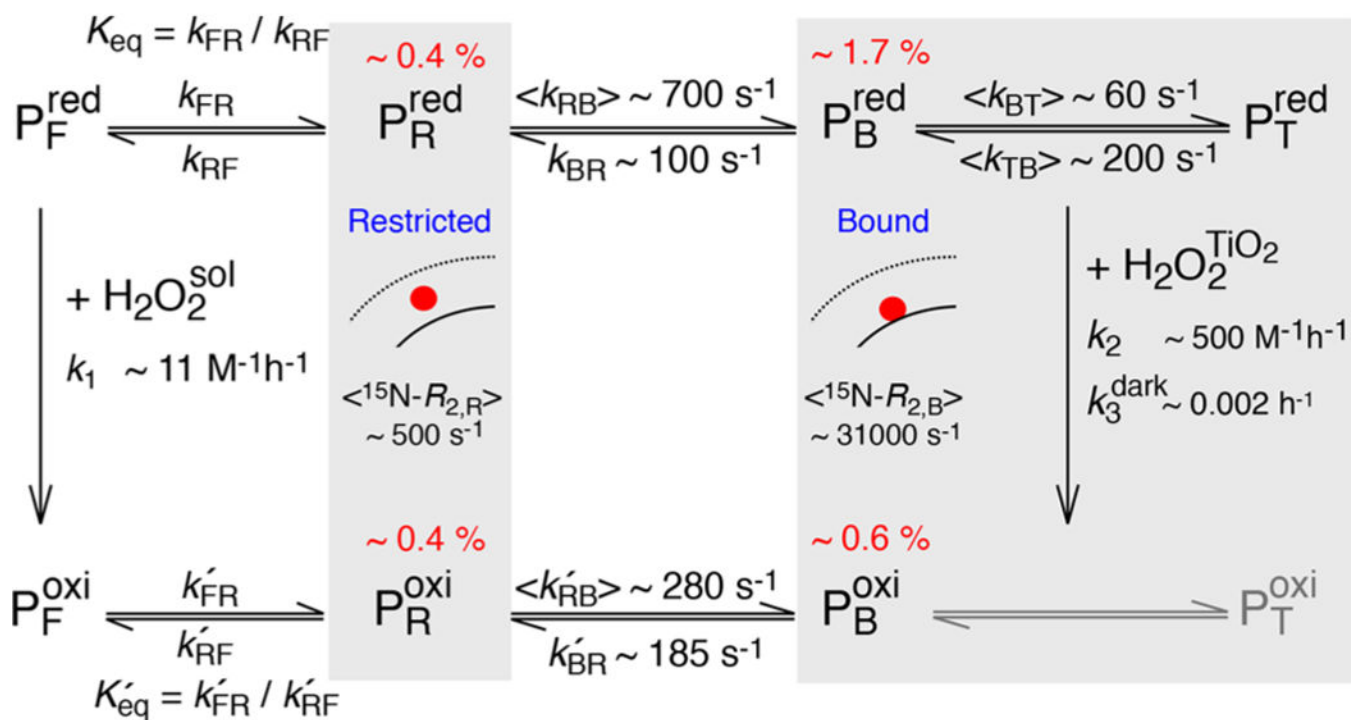
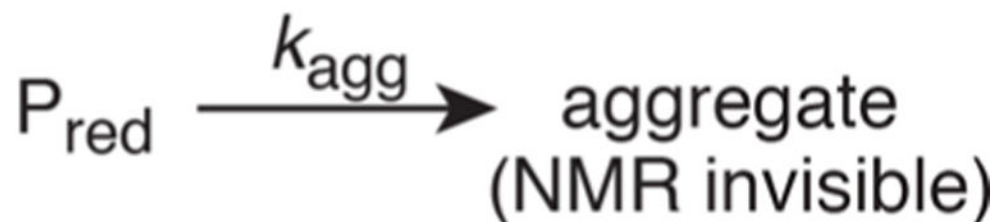
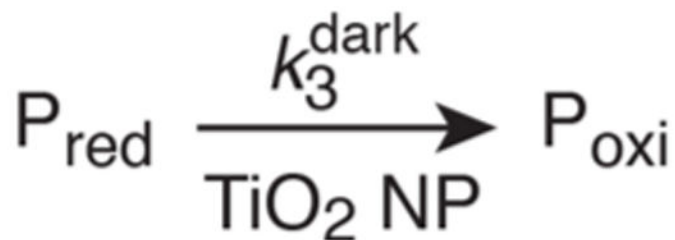
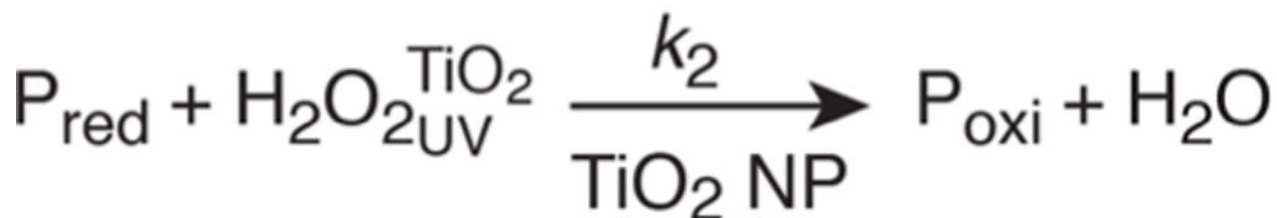
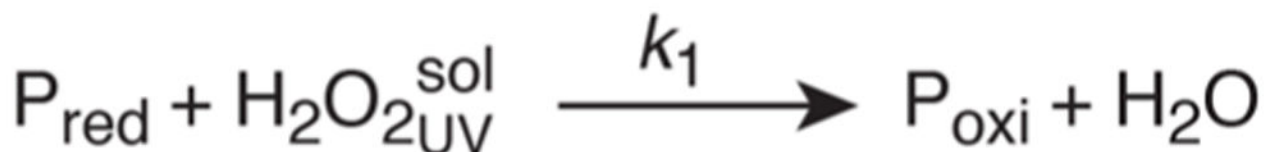


Figure 4. Overall kinetic scheme for the binding htt^{NT} to TiO₂ NPs coupled with oxidation of htt^{NT} to the Met⁷ sulfoxide form either in solution or on the NP surface. States in contact with TiO₂ NPs are shaded.

Aggregation



Oxidation (NMR visible)



Scheme 1.

Parallel Reactions Describing Aggregation and TiO₂ NP-Catalyzed Oxidation of htt^{NTQ_n} Peptides